Supporting Information

Ligand Effects on Electronic Structure and Bonding in U(III) Coordination Complexes: A Combined MCD, EPR and Computational Study

Nikki J. Wolford[a†], Xiaojuan Yu[b†], Suzanne C. Bart[c], Jochen Autschbach[b]*, Michael L. Neidig[a]*

[a] Department of Chemistry, University of Rochester, Rochester, New York 14627, United States, E-mail: neidig@chem.rochester.edu

[b] Department of Chemistry, University at Buffalo, State University of New York, Buffalo, New York 14260, United States, E-mail: jochena@buffalo.edu

[c] Department of Chemistry, Purdue University, West Lafayette, Indiana 47907, United States, E-mail: sbart@purdue.edu

Table of Contents

1. Experimental....S1-S3
   1.1. General Considerations....S1
   1.2. Preparation of $UI_3(1,4\text{-dioxane})_{1.5}$....S1
   1.3. Preparation of $UI_3(THF)_4$....S1
   1.4. Preparation of KTp*....S1
   1.5. Preparation of Tp*UI_2 (**1**)....S1
   1.6. Preparation of Tp*$_2$UI (**2**)....S1
   1.7. Preparation of Tp*$_2$UBn (**3**)....S2
   1.8. Preparation of Tp*$_2$UBipy (**4**)....S2
   1.9. Electronic Absorption....S2
   1.10. Electron Paramagnetic Resonance....S3
   1.11. Magnetic Circular Dichroism....S3
2. Field Dependent NIR and UV-vis MCD spectra (Figure S1)....S4
3. Temperature Dependent NIR and UV-vis MCD spectra (Figure S2)....S5
4. Computational Details....S6
   4.1. Table S1....S7
   4.2. Table S2....S8
   4.3. Table S3....S9
   4.4. Figure S3....S10
   4.5. Figure S4....S11
   4.6. Figure S5....S12-S13
   4.7. Figure S6....S14
   4.8. Figure S7....S15-S19
   4.9. Figure S8....S19
   4.10. Optimized Coordinates....S20-S25
5. Table of EPR g-values for U(III) complexes....S26
6. References....S27-S29

1. Experimental

1.1: General Considerations: All reactions, with the exception of the KTp* synthesis, were carried out in an MBraun insert atmosphere glovebox.

1.2: Preparation of UI_3(1,4-dioxane)$_{1.5}$: UI_3(1,4-dioxane)$_{1.5}$ was synthesized using a previously reported procedure. A 20 mL scintillation vial was charged with a stir bar, uranium turnings (2.50 g, 10.5 mmol), iodine (3.60 g, 14.2 mmol), and dioxane (10 mL). The reaction was stirred at RT for 18 h resulting in change in color from a brick red suspension to a dark blue/violet suspension. The reaction was filtered through a 50 mL medium-porosity fritted filter and the blue/violet solid collected. A spatula was used to remove the solid from the flask as it was quite sticky. The solid was washed with Et_2O (15 mL) and dried under reduced pressure. Once dry, the solid was examined and any residual turnings were removed using tweezers.

1.3: Preparation of $UI_3(THF)_4$: $UI_3(THF)_4$ was synthesized using a previously reported procedure. A 20 mL scintillation vial was charged with a stir bar, UI_3(1,4-dioxane)$_{1.5}$ (0.300 mg, 0.4 mmol) and THF (10 mL) resulting in a blue solution. The solution was stirred at RT. The solvent was removed under reduced pressure to yield $UI_3(THF)_4$ as a dark blue solid.

1.4: Preparation of KTp*: KTp* was synthesized using a previously reported procedure. A 100 mL round bottom flask was charged with potassium borohydride (0.70 g, 13 mmol) and 3,5-dimethylpyrazole (5 g, 52 mmol). The reaction was heated to melt at 250 °C under reflux conditions for 4 hours. After this time the reaction was allowed to cool until the melt solidified. Hot toluene (25mL) was added to the flask and decanted into a Büchner funnel. The solids were then washed on the filter with hot toluene (2x25mL). The solids were then dried under reduced pressure followed by purification by sublimation at 130 °C for ~6 hours. Purity was confirmed by NMR in D_2O.

1.5: Preparation of Tp*UI_2 (1)[1]: Tp*UI_2 was synthesized using a modified literature procedure. A 20 mL scintillation vial was charged with $UI_3(THF)_4$ (100 mg, 0.11 mmol) and 8mL THF. A second 20 mL vial was charged with KTp* (37 mg, 0.11 mmol) and 1 mL THF. The KTp* solution was added to the stirring solution of $UI_3(THF)_4$ dropwise at RT. The reaction was allowed to stir at RT for 3 hours. The solution was then filtered through celite into a clean 20 mL scintillation vial and solvent removed under reduced pressure. The blue solid was washed with pentane (3x 10 mL), dried, and stored at -30 °C for longevity.

1.6: Preparation of Tp*$_2$UI (2)[2]: Tp*$_2$UI was synthesized using a modified literature procedure. A 20 mL scintillation vial was charged with $UI_3(THF)_4$ (500 mg, 0.55 mmol) and 3mL THF. A second 20 mL vial was charged with KTp* (390 mg, 1.16 mmol) and 3 mL THF. The KTp* solution was added to the stirring solution of $UI_3(THF)_4$ dropwise at RT. The reaction was allowed to stir at RT for 3 hours resulting in a slight color change from blue/purple to purple. The solution was then filtered through celite into a clean 20 mL scintillation vial and solvent removed under reduced pressure. The solid was then washed with pentane. This was

done by adding 15 mL of pentane to the 20 mL vial which resulted in a suspension of purple solid and a green solution. Using a large pipet, the solid and solution were transferred to a pipette celite filter where the green solution was filtered off, leaving the blue solid on the celite. This solid was then washed with pentane (10 mL) by adding small amounts of pentane to the end of the pipette filter until no green was observed coming through the filter. The blue solid on the celite was then dissolved in THF through the filter by adding small amount of THF to the end of the pipette until all solid was dissolved. The THF solution was collected in a 20 mL scintillation vial and solvent removed under reduced pressure. The dry purple solid was stored at -30 °C for longevity.

1.7: Preparation of Tp*$_2$UBn (3)[3]: Tp*$_2$UBn was synthesized using a modified literature procedure. A 20 mL scintillation vial was charged with Tp*$_2$UI (100 mg, 0.10 mmol) and 2 mL Et_2O. A separate 20 mL vial was charged with KBn (7.2 mg, 0.110 mmol) and 5 mL THF. Both solutions were cooled to -25 °C. At this reduced temperature, the KBn solution was added to the stirring Tp*$_2$UI solution dropwise over the course of 5 minutes. The reaction was then warmed to RT where it was allowed to stir for 4 h resulting in a color change from purple to emerald green. The solution was filtered through celite and the solvent was removed under reduced pressure. The solid was then washed with pentane. This was done by adding 15 mL of pentane to the 20 mL vial which resulted in a suspension of green solid and a green solution. Using a large pipet, the solid and solution were transferred to a pipette celite filter where the green solution was filtered off, leaving the green solid on the celite. This solid was then washed with pentane (10 mL) by adding small amounts of pentane to the end of the pipette filter until no green was observed coming through the filter. The green solid on the celite was then dissolved in THF through the filter by adding small amount of THF to the end of the pipette until all solid was dissolved. The THF solution was collected in a 20 mL scintillation vial and solvent removed under reduced pressure. The dry green solid was stored at -30 °C for longevity.

1.8: Preparation of Tp*$_2$UBipy (4)[4]: Tp*$_2$UBipy was synthesized using a previously reported procedure. A 20 mL scintillation vial was charged with Tp*$_2$UI (50 mg, 0.052 mmol) and 1.7 mL toluene. A separate 20 mL vial was charged with 2,2'-bypridine (8.1 mg, 0.052 mmol) and 1.7 mL toluene. The 2,2'-bypridine solution was added to the purple Tp*$_2$UI solution at RT all at once while stirring. No color change was observed. KC_8 (14 mg, 0.104 mmol) was weighed by difference and added to the stirring solution of Tp*$_2$UI and 2,2'-bypridine at RT. The reaction was left to stir at RT for 3 h resulting in a color change from blue to brown/red. The solution was filtered through celitre into a clean 20 mL scintillation vial and the solvent removed under reduced pressure. The solid was dissolved in a minimal amount of a 60:40 mixture of THF/Et_2O and stored at -30 °C resulting in the formation of dark brown block crystals. The crystals were collected on a 3 mL fine porosity frit, washed with pentane (10 mL), and stored at -30 °C for longevity.

1.9: Electronic Absorption: Samples were prepared in an MBraun inert atmosphere glovebox. A 1.5 mM solution of each complex was prepared using an anhydrous 6:1 toluene: benzene solvent mixture and placed in an airtight 1 cm cuvette which was additionally sealed using

silicon grease. Electronic absorption measurements were recorded at room temperature with an Agilent Cary 60 UV-vis spectrophotometer.

1.10: Electron Paramagnetic Resonance: Samples were prepared in an MBraun inert atmosphere glovebox. ~5 mg of each complex was placed in a 4mM medium-walled suprasil quartz solid EPR tube from Wilmad Labglass which have a cap for maintaining air-free conditions. Silicon grease was also used on the cap to assure a seal. X-band EPR spectra were recorded on a Bruker EMXplus spectrometer equipped with a 4119HS cavity and an Oxford ESR-900 helium flow cryostat. The instrumental parameters employed for all samples were as follows: 1mW power; time constant 41ms; modulation amplitude 8G; 9.38GHz; modulation frequency 100kHz.

1.11: Magnetic Circular Dichroism: MCD samples of 1-3 were prepared using EPR pure powder material. MCD samples of 4 were prepared using finely ground crystalline material. A small amount of the powdered material (est. 1 mg) was placed on a quartz disk. 1 drop of isopentane was added on top of the solid and a second quartz disk was used to sandwich the material. The disks were pushed together while making circular motions to disperse the material across the whole disk. The disks were then placed inside of a copper cell and the faceplate applied. The samples were placed in liquid nitrogen while still in the glovebox to avoid oxidation and stored in liquid nitrogen until run. Low temperature MCD experiments were conducted using two Jasco spectropolarimeters. Both instruments utilize a modified sample compartment incorporating focusing optics and an Oxford Instruments SM4000−7T superconducting magnet/cryostat. This setup permits measurements from 1.6 to 290 K with magnetic fields up to 7 T. A calibrated Cernox sensor directly inserted in the copper sample holder is used to measure the temperature at the sample to 0.001 K. UV−visible MCD spectra were collected using a Jasco J-715 spectropolarimeter and a shielded S- 20 photomultiplier tube. Near-infrared (NIR) data were collected with a Jasco J-730 spectropolarimeter and a liquid nitrogen cooled InSb detector. All MCD spectra were baseline-corrected against zero-field scans.

2. Field Dependent NIR and UV-vis MCD spectra

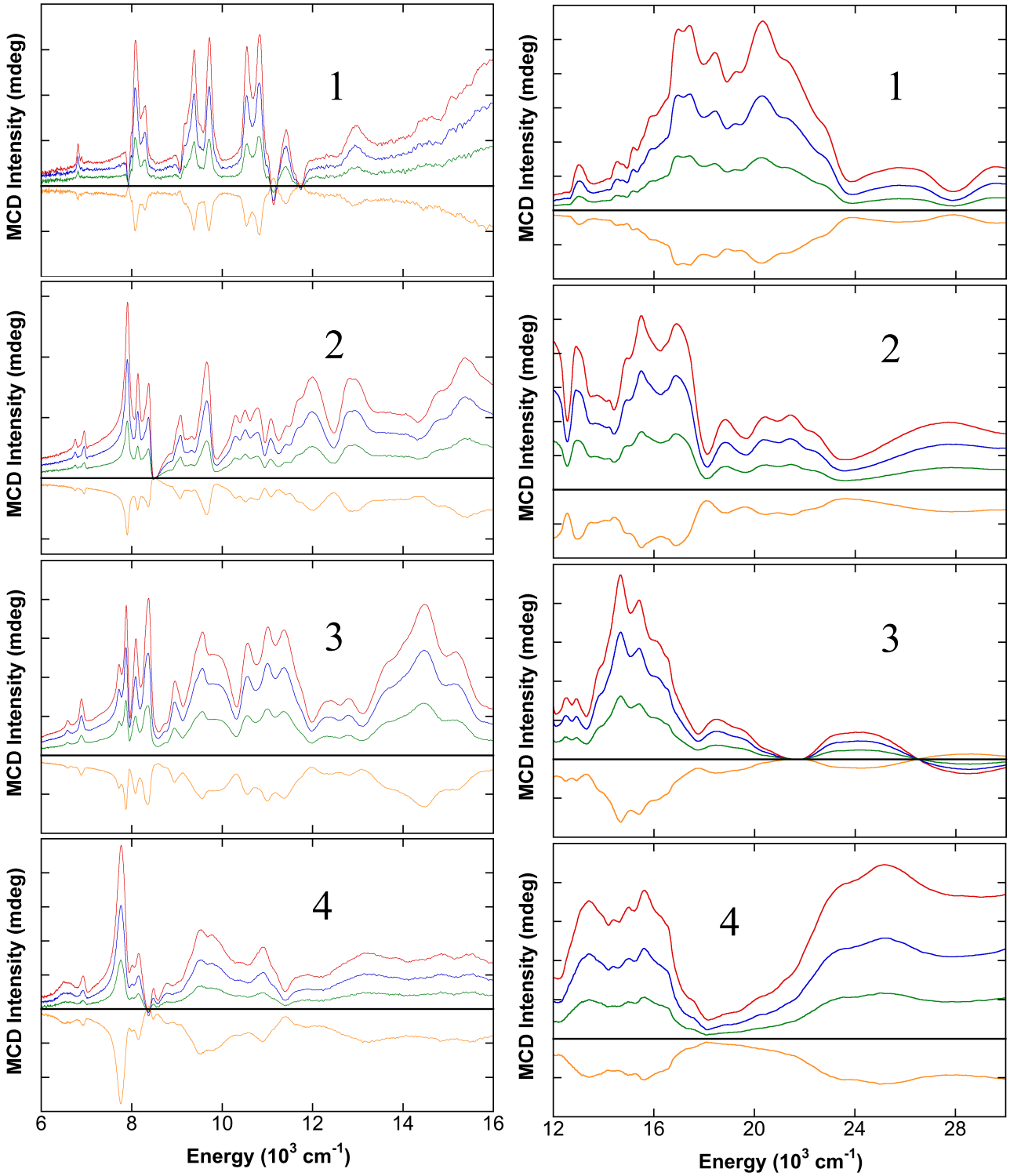

Figure S1: Field dependence of complexes **1-4**. Left, NIR energy region. Right, UV-vis energy region. 7 T (red), 3.5 T (blue), 1.5 T (green), -1.5 T (orange).

3. Temperature Dependent NIR and UV-vis MCD spectra

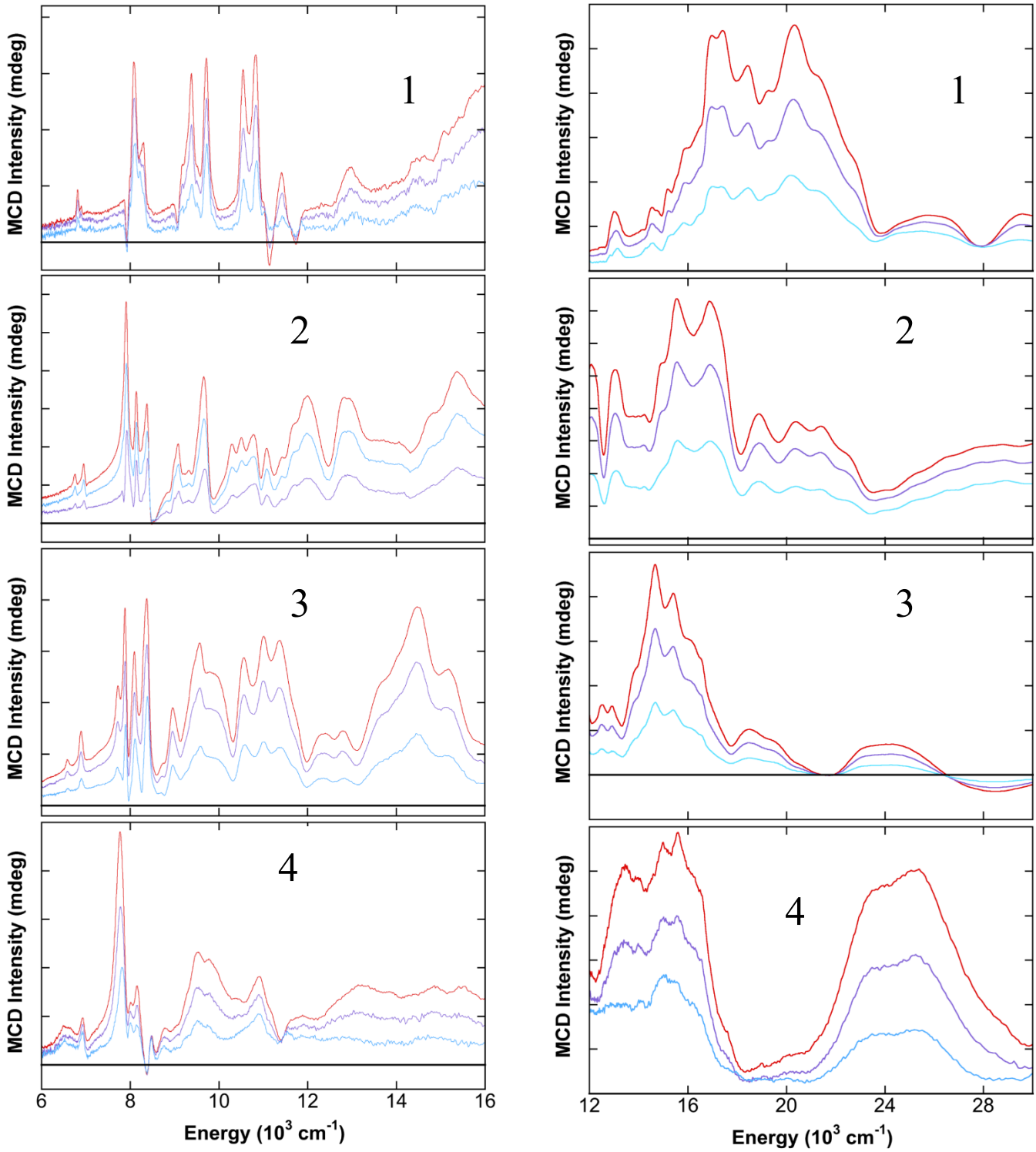

Figure S2: Temperature dependence of complexes **1**-**4**. Left, NIR energy region. Right, UV-vis energy region. 5 K (red), 10 K (purple), 25 K (blue).

4. Computational details:

Kohn-Sham density functional theory (DFT) calculations were performed on the target compounds [Tp*UI_2] (**1**), [Tp*$_2$UI] (**2**), [Tp*$_2$UBn] (**3**) and [Tp*$_2$UBipy] (**4**) with the Amsterdam Density Functional package (ADF, v2017).[5] The crystal structures were optimized for hydrogen positions using the Perdew–Burke–Ernzerhof (PBE) exchange-correlation functional and the all-electron scalar-relativistic Zeroth-Order Regular Approximation (ZORA) Hamiltonian.[6-8]An atom-pairwise correction for dispersion forces was considered (D3 with the Becke-Johnson damping).[9] For computational efficiency, methyl groups were replaced by hydrogen atoms. For U, N, O, and I, triple-ζ doubly polarized (TZ2P) Slater-type basis sets were employed, while singly polarized (TZP) basis sets were used for other atoms (B, C, H).[10] The extent of metal-ligand bonding was determined from natural localized molecular orbitals (NLMOs) analyses generated with NBO6.[11] The conductor-like screening model (COSMO) was applied to treat solvent effects (toluene).[12] The ground states of complexes **1**, **2** and **3** were determined as M_S = 3/2 spin quartet components, with minimal spin contamination: The expectation values of $\langle S^2 \rangle$ of complexes **1**, **2** and **3** were 3.757, 3.756, and 3.756, respectively (idealized: 3.75). The electronic absorption spectra of complexes **1**-**3** were calculated with time-dependent DFT (TD-DFT) linear response theory as implemented in ADF. A total number of 150 spin-allowed excited states were calculated for each complex. In order to assign the spectra, transitions with appreciable oscillator strength were analyzed in terms of donor—acceptor natural transition orbitals (NTO).[13]

To determine the ground state of complex **4**, spin-flip excitation calculations were performed.[14,15] Starting from the spin quintet M_S = 2 component, with the three unpaired electrons at uranium and the unpaired electron in the bipyridine ligand all having α spin, the energy for the transition to the lowest spin triplet state was negative (-6.7 eV, PBE/ALDA), indicating that the ground state of **4** is a spin triplet, in which the unpaired electron in the ligand is antiferromagnetically coupled to the unpaired electrons at uranium. The electronic excitations in this complex exhibited pronounced charge-transfer character. Therefore, the TD-DFT calculations utilized the range-separated hybrid functional CAM-B3LYP[16] and the Tamm-Dancoff approximation[17] as implemented in ORCA.[18,19] Starting from a spin triplet reference (CAM-B3LYP: $\langle S^2 \rangle$=2.98; with ADF and PBE the value is 2.78. Both indicate strong spin contamination, reflecting the multi-configurational character of the electronic state), a total number of 200 spin-allowed excited states were calculated. The conductor-like polarizable continuum model (CPCM) was applied to treat solvent effects (toluene).[20] For computational efficiency, the resolution-of-identity technique RIJCOSX in conjunction with the chain of spheres (COSX) approximation for the Hartree-Fock exchange were used in these calculations.[21]

Ab initio wave function calculations were performed with a developer's version of the OpenMolcas package based on Molcas release 8.[22,23] The 2nd-order Douglas-Kroll-Hess scalar relativistic Hamiltonian[24] was employed in the calculations without Spin-orbit (SO) coupling, in conjunction with all-electron atomic natural orbital relativistically contracted basis sets (Np, I = ANO-RCC-VTZP; C, B, N = ANO-RCC-VDZP; H = ANO-RCC-MB). The Complete Active Space Self Consistent Field method (CASSCF) was used to introduce mostly static

correlation. The computations used state averaged CASSCF wave functions.[25] The CAS calculations were performed using a minimal active space CAS(3,7) containing the seven 5*f* orbitals. SO coupling was treated by state interactions between the CASSCF wavefunctions, using the Restricted Active Space State Interaction (RASSI) program. State-averaged CAS calculations in the present work were performed for all the quartet (35 roots) and all of the doublet (112 roots) of the U^{3+} $5f$ manifold were determined and coupled in the SO-RASSI step for the complexes **1-3**. The SO operator matrix was calculated from atomic mean-field (AMFI) SO integrals. The wavefunction components used for the analysis diagonalize the projection of the operator $\hat{L} + g_e\hat{S}$ onto the direction of the magnetic axes (principal axes of the *g*-matrix). Graphical visualizations of the associated natural spin orbitals (NSOs), spin and orbital magnetization density were created with the graphical user interface of the ADF suite.[5]

4.1:

Table **S1**. The calculated relative energies at the CAS-SO level between the ground state (GS) and low-lying excited states (ESs) for complexes **1-3**. The states are assigned based on their free ion term and level parentage.

Complex	CASSCF-SR	Energy (cm^{-1})	CASSCF-SO	Energy (cm^{-1})
1	^4I	0-1454	$^4I_{9/2}$	0-613
			$^4I_{11/2}$	4380-4729
			$^4I_{13/2}$	8372-8833
			$^4I_{15/2}$	11222-12665
	SO GS: 89% ^4I+7% ^2H			
2	^4I	0-1457	$^4I_{9/2}$	0-733
			$^4I_{11/2}$	4416-4882
			$^4I_{13/2}$	8340-8926
			$^4I_{15/2}$	11073-12590
	SO GS: 88% ^4I+8% ^2H			
3	^4I	0-1639	$^4I_{9/2}$	0-811
			$^4I_{11/2}$	4348-4921
			$^4I_{13/2}$	8226-8938
			$^4I_{15/2}$	10843-12520
	SO GS: 87% ^4I+6% ^2H			

4.2:

Table **S2**. Spin and angular momentum expectation values and *g*-factors (absolute values) from CAS(3,7)-SO calculations for complex **1**-**3**.

	1	**2**	**3**
$\langle L_X \rangle$	-0.077	-0.745	-0.469
$\langle L_Y \rangle$	-0.706	-0.933	-0.929
$\langle L_Z \rangle$	-4.350	-3.890	-4.143
$\langle S_X \rangle$	0.002	0.146	0.064
$\langle S_Y \rangle$	0.151	0.181	0.210
$\langle S_Z \rangle$	0.965	0.893	0.933
g_X	0.15	0.90	0.68
g_Y	0.81	1.14	1.01
g_Z	4.84	4.20	4.55

4.3:

Table **S3**. Charges and natural electron configuration on the uranium cation for complexes **1-4**, from scalar relativistic DFT and NBO calculations.

uranium	Natural charge	Natural electron configuration
1	1.26	[core]7s(0.23) 5f(3.31) 6d(1.02) 7p(0.01)
2	1.37	[core]7s(0.20) 5f(3.31) 6d(0.96) 7p(0.01)
3	1.71	[core]7s(0.17) 5f(3.23) 6d(0.78) 7p(0.02)
4	1.60	[core]7s(0.16) 5f(3.21) 6d(0.81) 7p(0.02)

4.4:

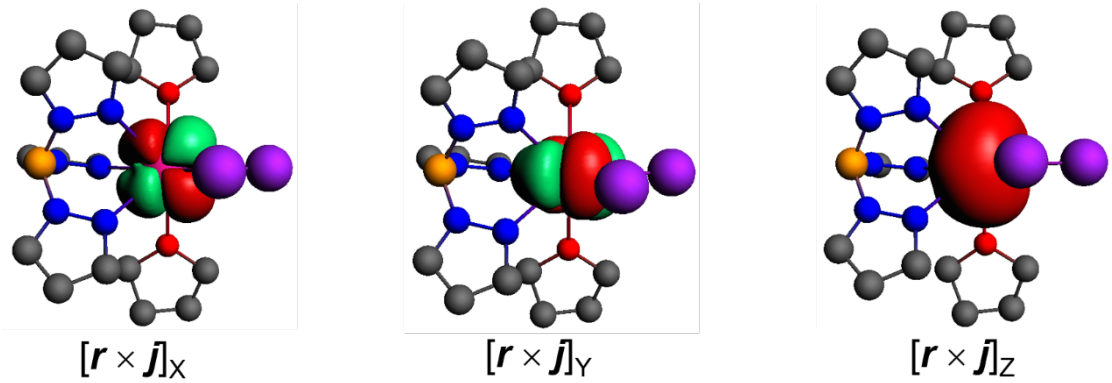

Figure **S3**. Isosurfaces (±0.001 au) for the components of the orbital magnetization $m_u=[\boldsymbol{r}\times\boldsymbol{j}]_u$ from ab-initio SO(3,7)-CAS calculation for magnetization quantization axis Z.

4.5:

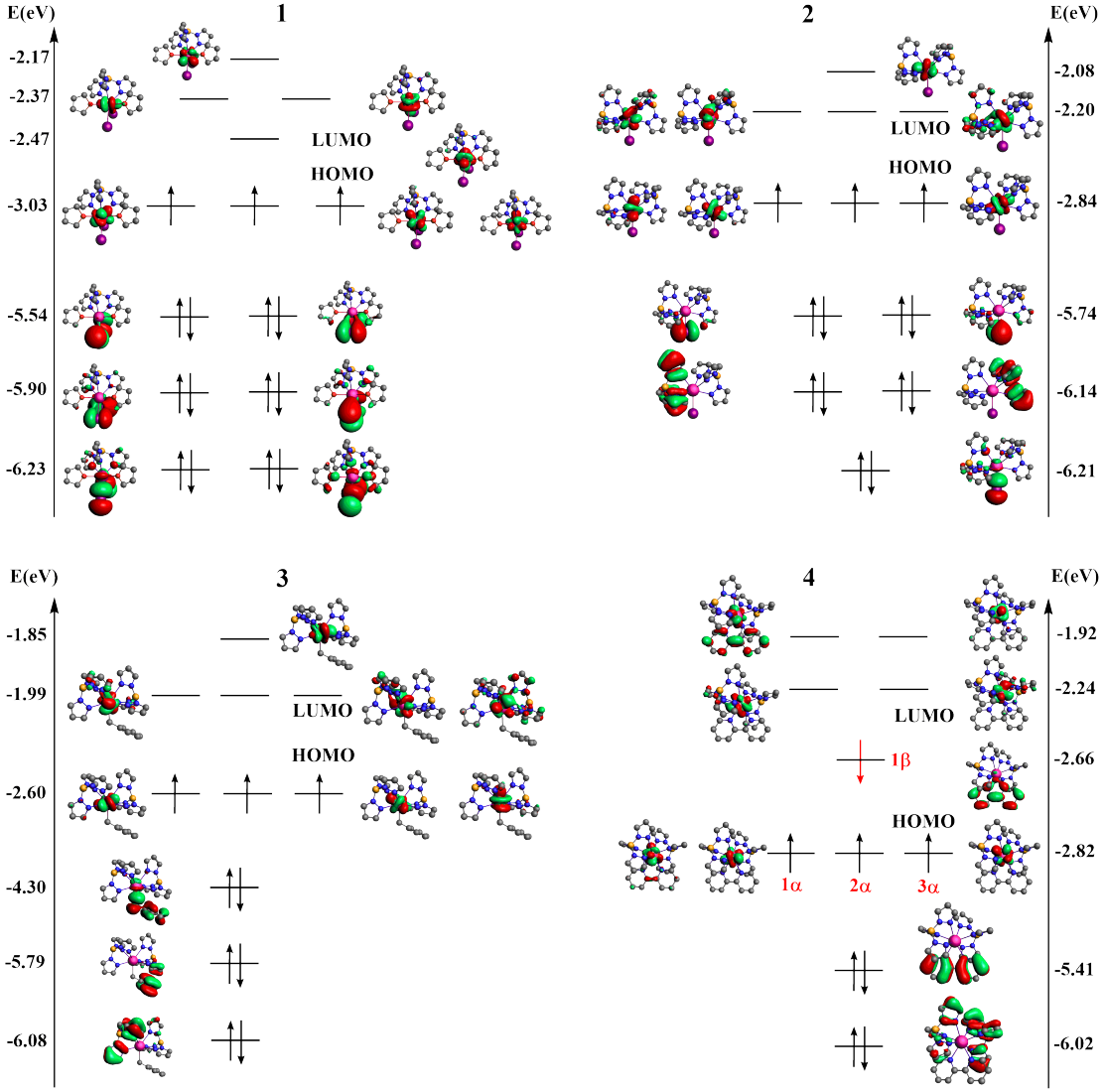

Figure **S4.** MO diagrams obtained with all-electron scalar relativistic DFT for the complexes **1-4**. Shown are the α spin MOs and their energies. (Canonical MO isosurfaces at ±0.03 au. Hydrogen atoms are omitted for clarity).

4.6:

1

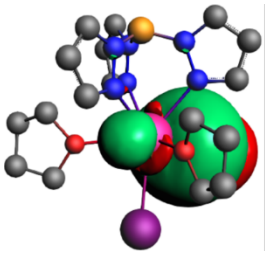

2×σ(U-I)
88% I (41 s; 59 p)
12% U (28 s; 56 d; 16 f)

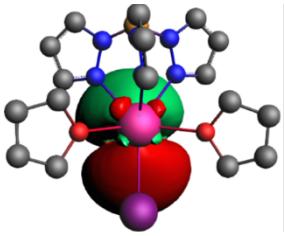

2×π(U-I)
94% I (100 p)
6% U (61 d; 39 f)

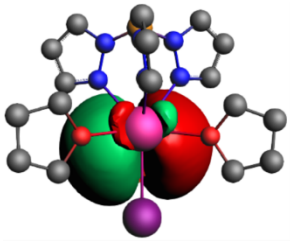

2×π(U-I)
94% I (100 p)
6% U (65 d; 35 f)

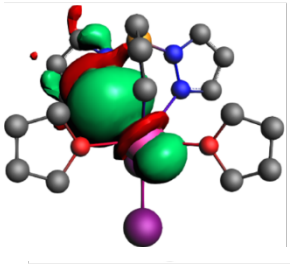

3×σ(U-N)
90% N (40 s; 60 p)
8% U (13 s; 55 d; 32 f)

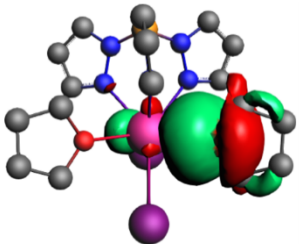

2×σ(U-O)
94% O (47 s; 53 p)
4% U (17 s; 53 d; 30 f)

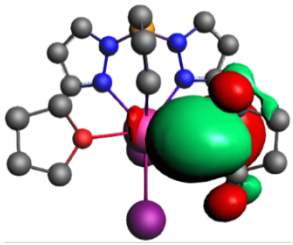

2×π(U-O)
95% O (100 p)
2% U (38 d; 62 f)

2

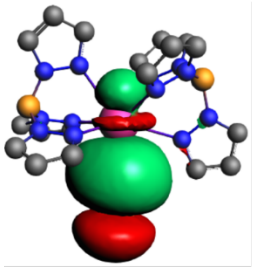

σ(U-I)
87% I (40 s; 60 p)
13% U (25 s; 60 d; 15 f)

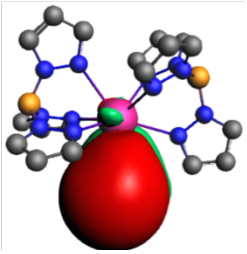

π(U-I)
93% I (100 p)
7% U (64 d; 36 f)

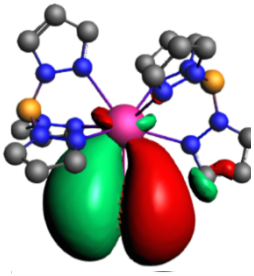

π(U-I)
93% I (100 p)
6% U (55 d; 45 f)

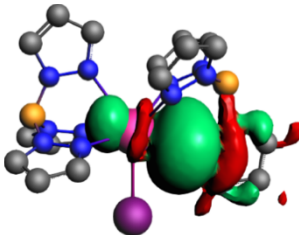

6×σ(U-N)
90% N (40 s; 60 p)
8% U (13 s; 56 d; 31 f)

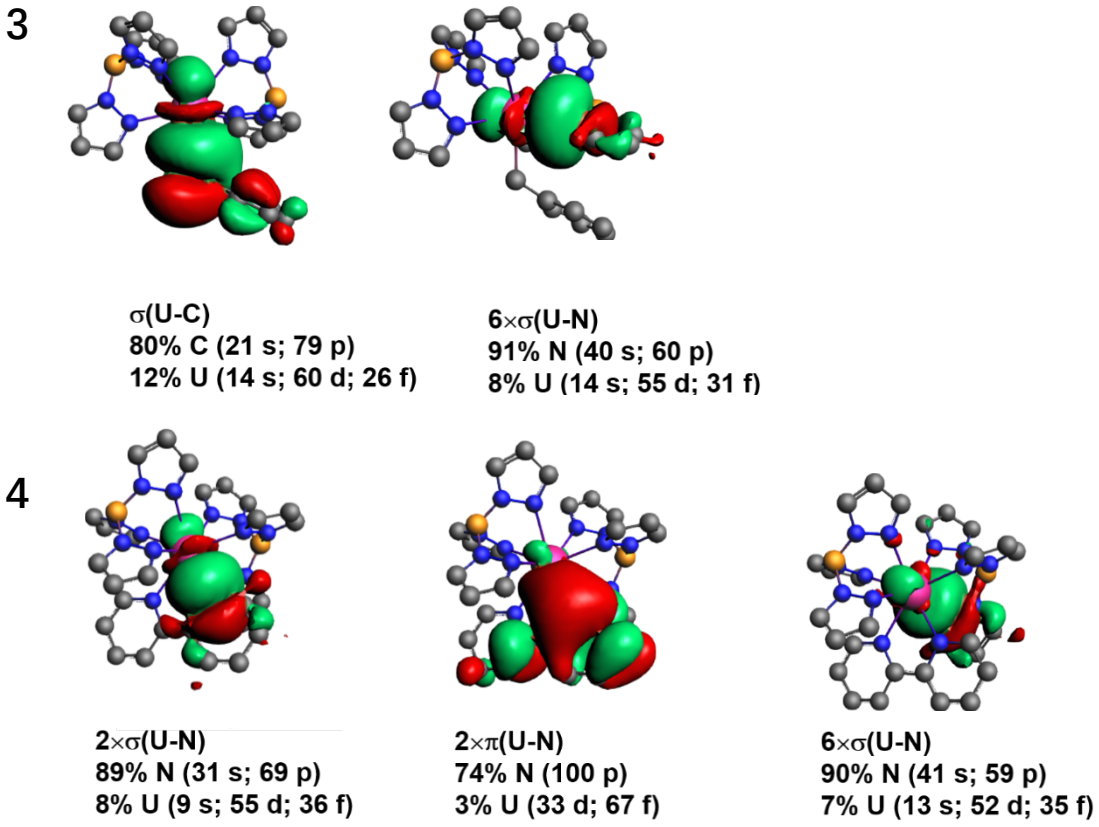

Figure **S5.** Bonding U-ligand natural localized molecular orbitals (NLMOs) for the complexes **1-4** (isosurfaces at ±0.01 au. Hydrogen atoms are omitted for clarity). The the α spin NLMOs are shown. Weight percentages from U and ligand center shown below the graphics are averaged over spins.

4.7:

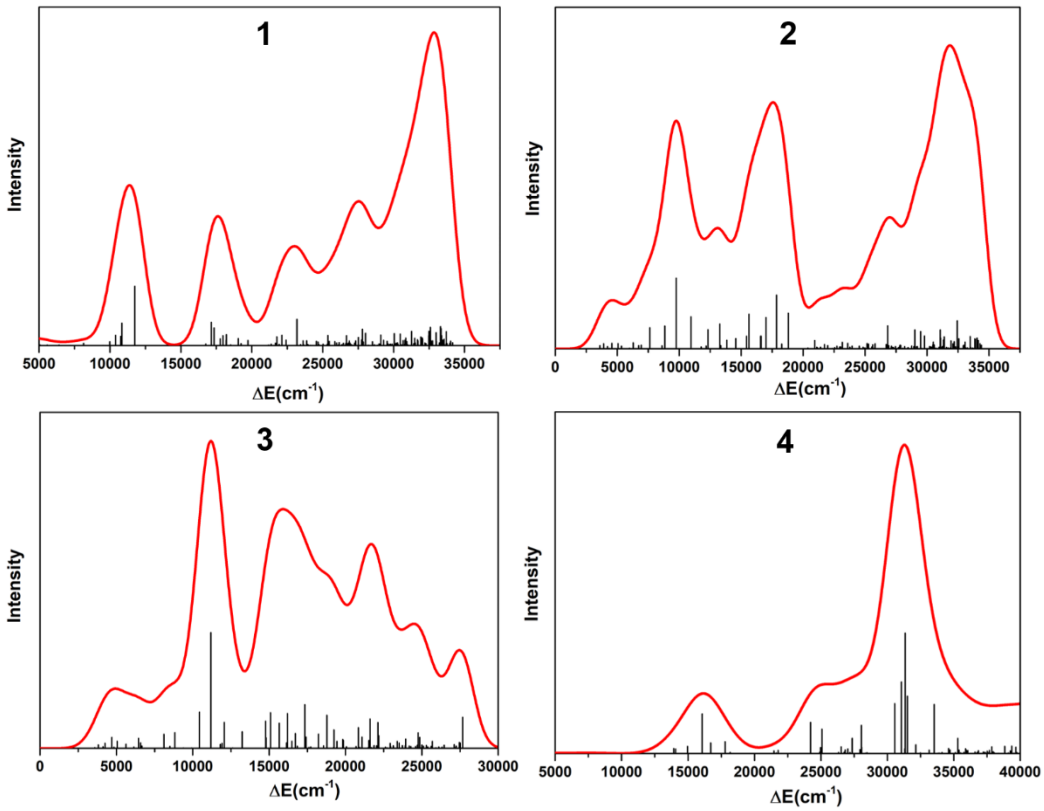

Figure **S6**. TD-DFT spectra of complexes **1-4**. Gaussian broadening of the calculated transitions for 0-35000 cm^{-1}, 0-35000 cm^{-1}, 0-30000 cm^{-1} and 0-40000 cm^{-1}, respectively. The "stick spectra" represent the relative magnitudes of the calculated oscillator strengths.

4.8:

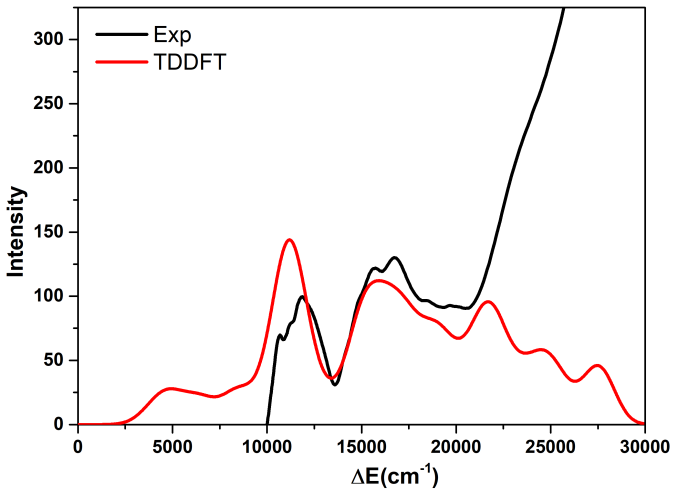

Figure **S7**. TD-DFT spectra (red) and experimental EAS spectra (black) of complex **3.**

4.9: Figure S8

Complex **1**:

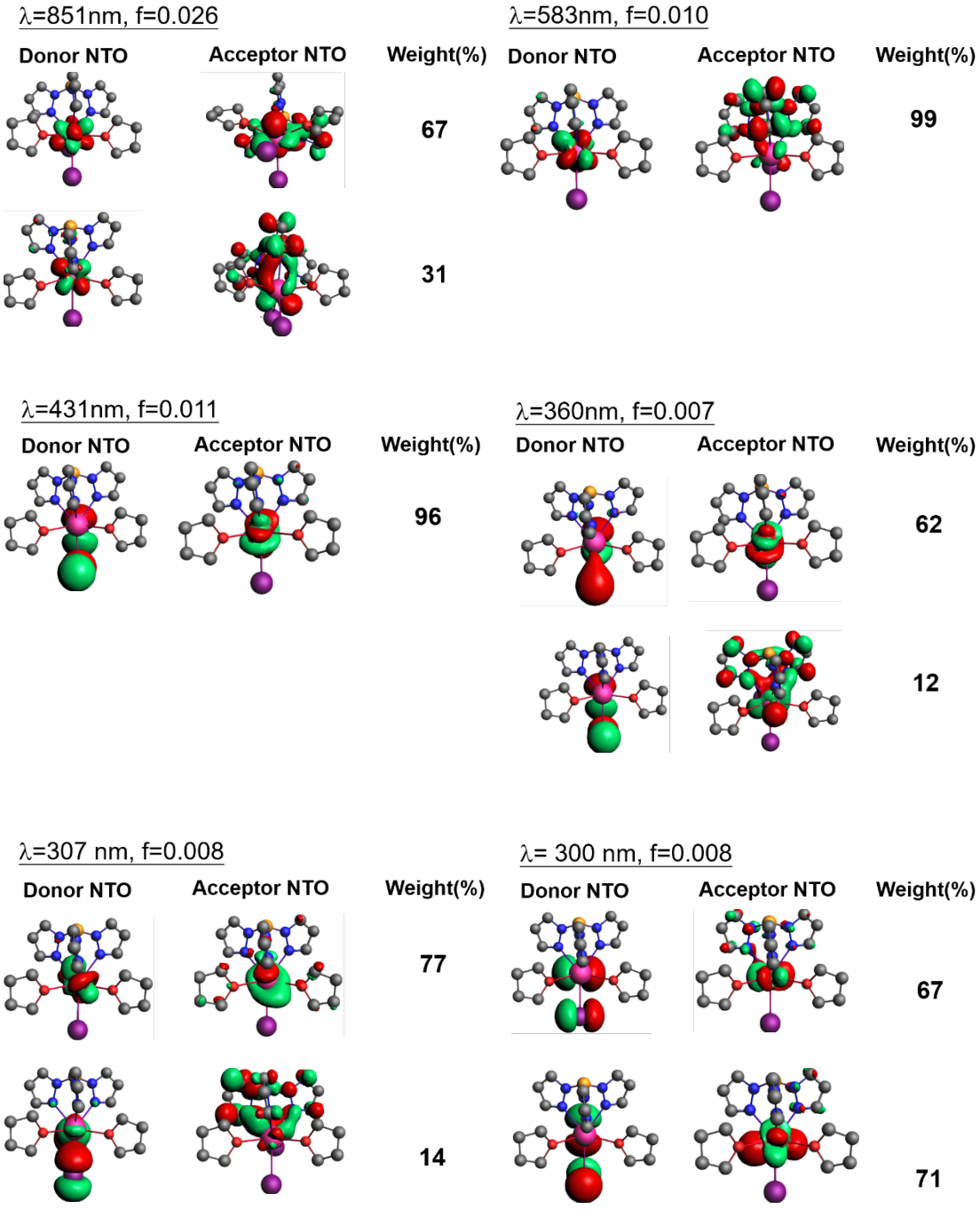

Complex **2**:

λ=2193nm, f=0.0015

Donor NTO	Acceptor NTO	Weight(%)
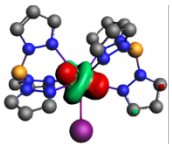	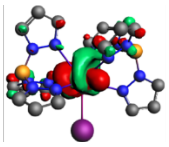	75
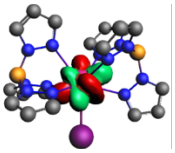	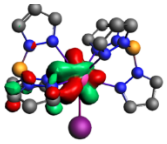	24

λ=1970nm, f=0.0016

Donor NTO	Acceptor NTO	Weight(%)
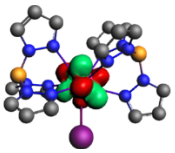	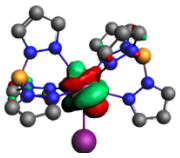	85
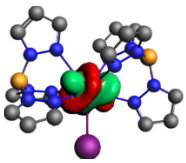	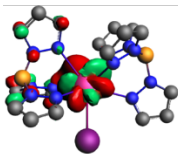	11

λ=1023nm, f=0.021

Donor NTO	Acceptor NTO	Weight(%)
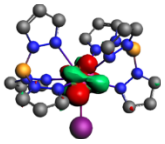	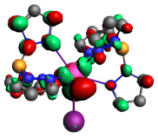	98

λ=559nm, f=0.016

Donor NTO	Acceptor NTO	Weight(%)
	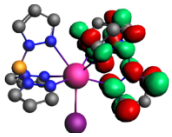	99

λ=640nm, f=0.010

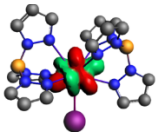	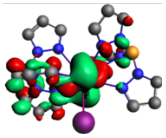	78
	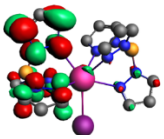	20

λ=531nm, f=0.010

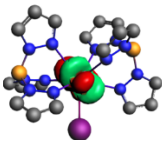	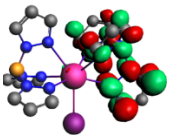	94

λ=373nm, f=0.006

Donor NTO	Acceptor NTO	Weight(%)
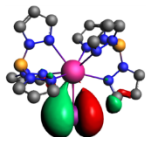	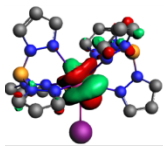	71
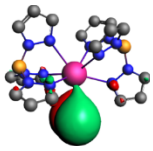	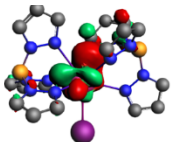	26

λ=345nm, f=0.005

Donor NTO	Acceptor NTO	Weight(%)
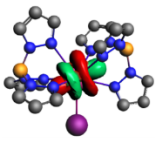	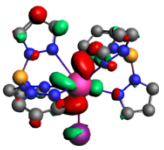	93

λ=322nm, f=0.006

Donor NTO	Acceptor NTO	Weight(%)
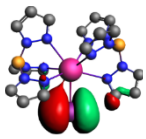		66
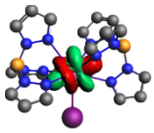	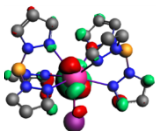	23

λ=308nm, f=0.008

Donor NTO	Acceptor NTO	Weight(%)
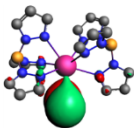	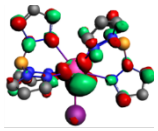	75
		16

Complex **3**:

λ=894 nm, f=0.036

Donor NTO	Acceptor NTO	Weight(%)
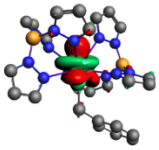	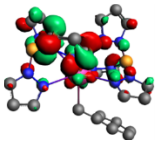	94

λ=662 nm, f=0.011

Donor NTO	Acceptor NTO	Weight(%)
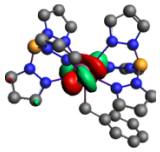	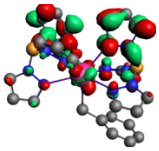	77

λ=463 nm, f=0.009

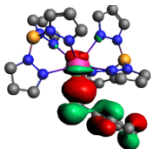	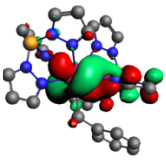	88
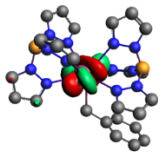	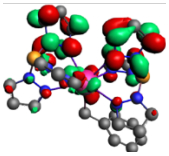	22

Complex **4**:

λ= 718 nm, f=0.006

Donor NTO	Acceptor NTO	Weight(%)
	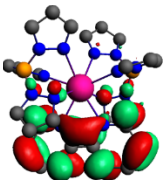	80
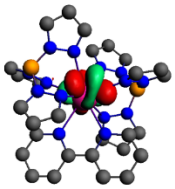	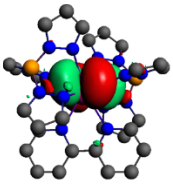	16

λ= 711 nm, f=0.005

Donor NTO	Acceptor NTO	Weight(%)
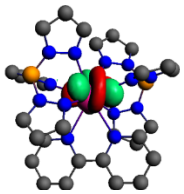	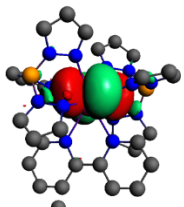	81
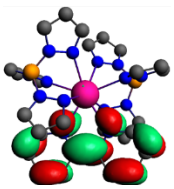	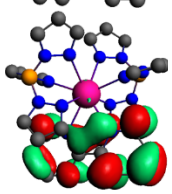	17

λ= 669 nm, f=0.008

Donor NTO	Acceptor NTO	Weight(%)
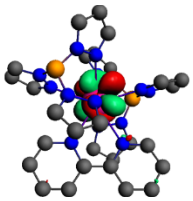	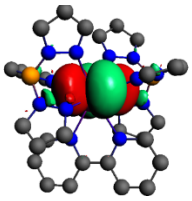	98

λ= 598 nm, f=0.012

Donor NTO	Acceptor NTO	Weight(%)
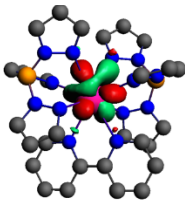	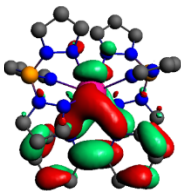	99

λ= 623 nm, f=0.046

Donor NTO	Acceptor NTO	Weight(%)
	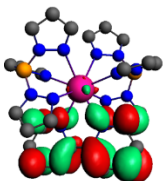	91

λ= 562 nm, f=0.014

Donor NTO	Acceptor NTO	Weight(%)
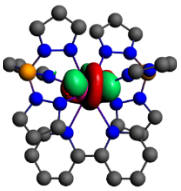	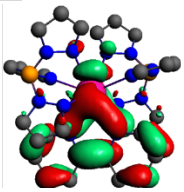	99

λ= 413 nm, f=0.036

Donor NTO	Acceptor NTO	Weight(%)
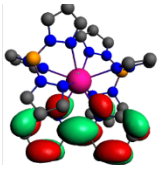	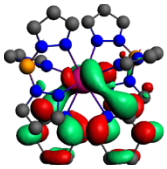	85

λ= 357 nm, f=0.033

Donor NTO	Acceptor NTO	Weight(%)
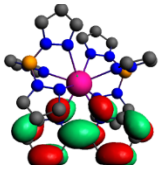	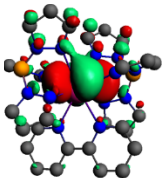	63
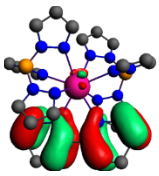	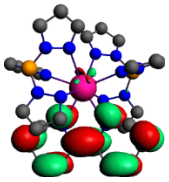	18

λ= 327 nm, f=0.059

Donor NTO	Acceptor NTO	Weight(%)
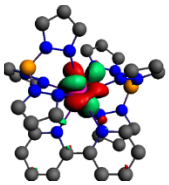	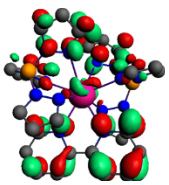	54
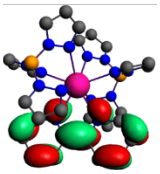	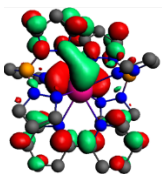	18

λ= 322 nm, f=0.084

Donor NTO	Acceptor NTO	Weight(%)
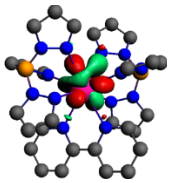	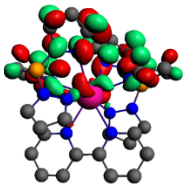	48
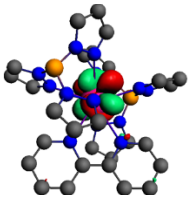	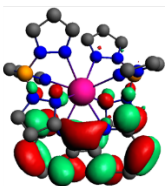	28

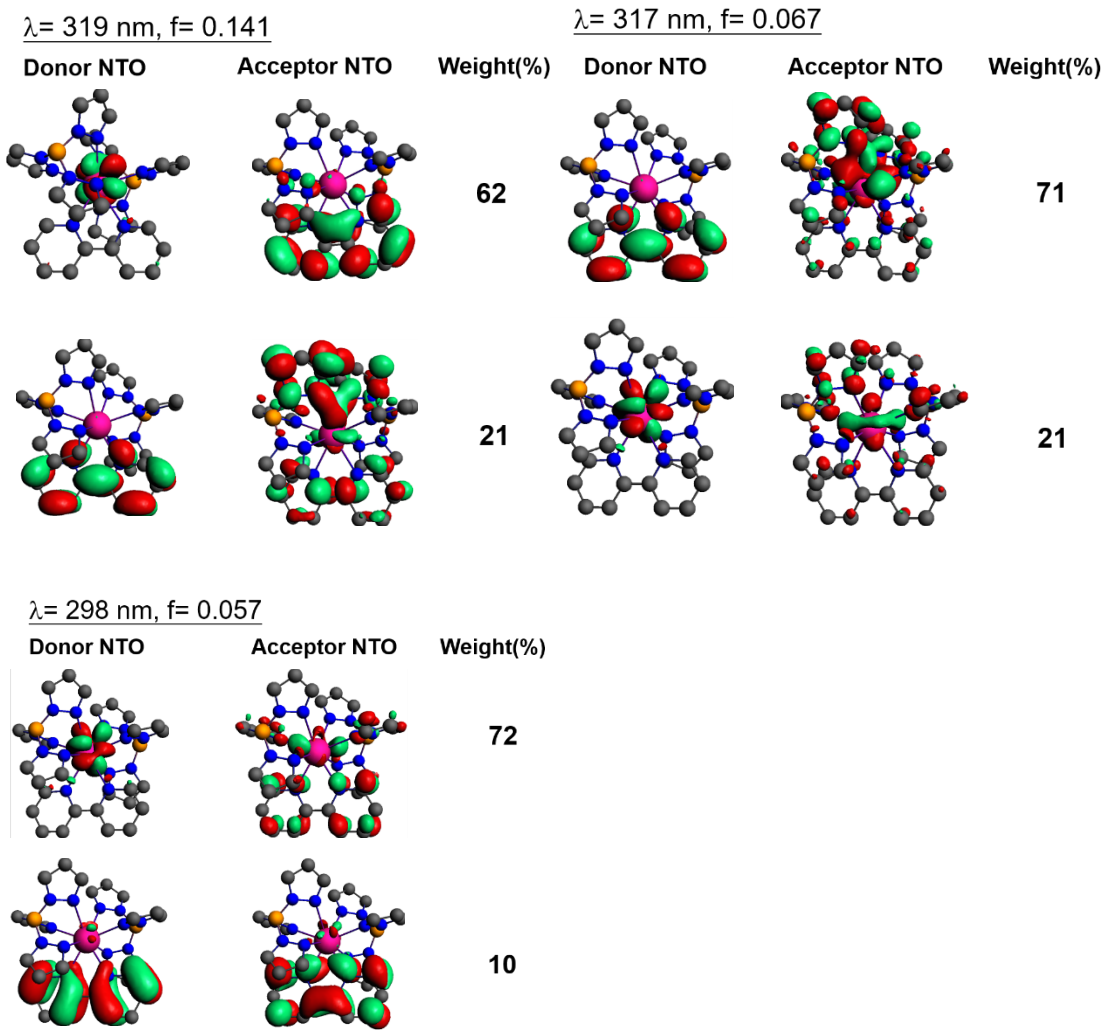

Figure **S8**. Natural transition orbital (NTO) analysis for complexes **1-4**. The oscillator strength (f) are given in length representation.

Table S4. Cartesian Coordinates of Complexes **1**-**4**.

Complex	**xyz**			
Tp*UI_2 (**1**)	U	7.701933	10.090425	2.894241
	I	10.603683	11.269302	2.904430
	I	7.251071	11.892164	0.295266
	O	7.346095	8.208320	1.163187
	O	5.725970	11.606172	3.691692
	N	7.935274	10.402101	5.385034
	N	7.833612	9.365864	6.285896
	N	5.921462	8.588054	3.911135
	N	6.090746	7.948191	5.119790
	N	8.934425	8.018233	3.763533
	N	8.523802	7.365498	4.905341
	C	7.997048	9.819298	7.553202
	C	8.210299	11.196593	7.482646
	C	8.150489	11.519258	6.123966
	C	4.934853	7.343524	5.474968
	C	4.006673	7.599808	4.486065
	C	4.660818	8.365025	3.530040
	C	9.151561	6.165167	5.014728
	C	10.010058	6.056480	3.939044
	C	9.865338	7.210620	3.192811
	C	6.964664	6.825522	1.466459
	C	7.271521	6.053065	0.266795
	C	7.216762	6.995217	-0.816957
	C	7.462267	8.309782	-0.279619
	C	5.223369	12.848820	3.110895
	C	4.275782	13.468316	4.061210
	C	4.461668	12.673649	5.361457
	C	4.883065	11.322254	4.865656
	B	7.444211	7.942601	5.836666
	H	7.358357	7.240039	6.814012
	H	8.383940	11.873420	8.313180
	H	2.976856	7.256414	4.459357
	H	10.680481	5.227520	3.731373
	H	7.505564	6.520700	2.367298
	H	5.888181	6.831029	1.699088
	H	8.282204	5.619023	0.362863
	H	6.587842	5.202122	0.147793
	H	6.217878	6.973075	-1.286256
	H	7.916212	6.751095	-1.628788
	H	6.758795	9.077885	-0.624821
	H	8.475991	8.688568	-0.484986

	H	4.770153	12.606416	2.140083
	H	6.105638	13.470987	2.910998
	H	3.239724	13.363273	3.709517
	H	4.468060	14.538600	4.203200
	H	5.260253	13.114019	5.976866
	H	3.548813	12.627839	5.968046
	H	5.485836	10.740585	5.567566
	H	4.024221	10.718491	4.535313
	H	8.283111	12.480471	5.635238
	H	7.950277	9.141188	8.398748
	H	8.958174	5.507533	5.855398
	H	10.364335	7.516036	2.277499
	H	4.861117	6.777270	6.397800
	H	4.283017	8.778630	2.598148
Tp^*_2UI (**2**)	U	11.508645	3.098038	-1.427217
	I	8.989341	4.685065	-0.858143
	N	12.019278	5.512239	-2.309039
	N	13.128989	5.814300	-3.050337
	N	13.958584	3.722280	-0.963815
	N	14.762810	4.285166	-1.925002
	N	12.552813	2.874457	-3.749633
	N	13.697651	3.564803	-4.105218
	N	12.617903	0.626767	-1.232911
	N	11.812449	-0.369405	-0.688438
	N	11.194310	2.193378	0.866854
	N	10.629040	0.964504	1.057417
	N	9.787339	1.371761	-2.091363
	N	9.490188	0.360548	-1.216395
	C	13.141160	7.082612	-3.417094
	C	12.008499	7.692359	-2.891764
	C	11.330946	6.684876	-2.225593
	C	16.051315	4.315076	-1.473511
	C	16.105693	3.761530	-0.222031
	C	14.763972	3.371399	0.044367
	C	14.237409	2.988908	-5.177042
	C	13.470543	1.917667	-5.586373
	C	12.463350	1.902693	-4.650866
	C	12.422178	-1.570133	-0.902384
	C	13.601987	-1.322580	-1.532285
	C	13.724064	0.013219	-1.701640
	C	10.379039	0.767473	2.389512
	C	10.789712	1.930626	3.061948
	C	11.260753	2.765532	2.094273
	C	8.345348	-0.269773	-1.599908

	C	7.891373	0.325094	-2.770984
	C	8.815229	1.319350	-3.042457
	B	14.235126	4.752343	-3.277682
	B	10.453871	-0.082247	-0.075818
	H	13.957614	7.486027	-4.008308
	H	11.710109	8.730162	-3.002673
	H	10.396890	6.733520	-1.681585
	H	16.832000	4.738599	-2.097942
	H	16.973789	3.627255	0.414257
	H	14.356680	2.882601	0.926426
	H	15.148204	3.398535	-5.606397
	H	13.632777	1.251457	-6.425568
	H	11.632815	1.200625	-4.580943
	H	14.329174	-2.078810	-1.819896
	H	10.728217	2.117698	4.129228
	H	7.011359	0.060000	-3.347610
	H	15.145738	5.254511	-3.890211
	H	10.006274	-1.088789	0.413994
	H	11.655424	3.774022	2.194325
	H	9.936393	-0.157458	2.742625
	H	11.966486	-2.496846	-0.568399
	H	14.511814	0.598717	-2.167526
	H	7.956489	-1.100689	-1.020396
	H	8.819745	2.044114	-3.853144
Tp^*_2UBn (**3**)	U	11.508566	3.098054	-1.427193
	N	12.019120	5.512278	-2.308995
	N	13.128806	5.814375	-3.050317
	N	13.958502	3.722347	-0.963844
	N	14.762690	4.285265	-1.925044
	N	12.552681	2.874529	-3.749638
	N	13.697493	3.564906	-4.105243
	N	12.617887	0.626806	-1.232948
	N	11.812470	-0.369392	-0.688469
	N	11.194310	2.193355	0.866874
	N	10.629074	0.964466	1.057434
	N	9.787284	1.371745	-2.091319
	N	9.490178	0.360514	-1.216357
	C	13.140937	7.082693	-3.417057
	C	12.008276	7.692407	-2.891690
	C	11.330763	6.684898	-2.225516
	C	16.051206	4.315199	-1.473585
	C	16.105628	3.761638	-0.222113
	C	14.763924	3.371471	0.044312
	C	14.237238	2.989039	-5.177088

	C	13.470387	1.917785	-5.586414
	C	12.463218	1.902775	-4.650882
	C	9.382931	4.373497	-0.788562
	C	8.326238	3.729990	0.115442
	C	7.281593	2.945853	-0.438061
	C	6.374696	2.253545	0.376736
	C	6.436344	2.352979	1.723739
	C	7.421788	3.112718	2.276243
	C	8.308185	3.752425	1.500744
	C	12.422222	-1.570103	-0.902446
	C	13.602009	-1.322513	-1.532373
	C	13.724050	0.013290	-1.701714
	C	10.379111	0.767411	2.389533
	C	10.789773	1.930564	3.061975
	C	11.260770	2.765494	2.094299
	C	8.345343	-0.269829	-1.599849
	C	7.891325	0.325043	-2.770906
	C	8.815151	1.319324	-3.042389
	B	14.234962	4.752448	-3.277704
	B	10.453900	-0.082274	-0.075810
	H	13.957681	7.488595	-4.005634
	H	11.710294	8.730190	-3.003928
	H	10.387996	6.726173	-1.689480
	H	16.832465	4.738961	-2.097254
	H	16.974811	3.626467	0.412783
	H	14.355259	2.884310	0.926671
	H	15.149780	3.396374	-5.605070
	H	13.634167	1.250613	-6.424650
	H	11.632864	1.200507	-4.580010
	H	8.942662	4.656989	-1.761218
	H	9.787329	5.279631	-0.301150
	H	7.200827	2.846234	-1.521877
	H	5.603873	1.644771	-0.104338
	H	5.719806	1.821594	2.355758
	H	7.500868	3.203310	3.363109
	H	9.081156	4.348820	1.998936
	H	14.328928	-2.079306	-1.819764
	H	10.722043	2.119378	4.128511
	H	7.009726	0.061549	-3.345754
	H	15.144337	5.256388	-3.891339
	H	10.006286	-1.090058	0.412763
	H	8.822977	2.039795	-3.857260
	H	7.953047	-1.096454	-1.016907
	H	11.967121	-2.497314	-0.568608

	H	14.511532	0.599710	-2.167011
	H	11.661806	3.771289	2.195155
	H	9.929593	-0.154292	2.741847
Tp*$_2$UBipy (**4**)	U	0.000000	0.000000	0.000000
	N	-2.568892	-0.626243	-0.105635
	N	-3.092321	0.611947	-0.430828
	N	-0.634251	2.493888	-0.343096
	N	-1.922151	2.870268	-0.094066
	N	-1.351062	0.844387	2.168729
	N	-2.573079	1.486066	1.906156
	N	0.253906	-2.232501	-1.289996
	N	-0.690361	0.023678	-2.470983
	N	0.757671	-1.670979	1.795289
	N	2.111579	-1.808755	2.031757
	N	2.434176	-0.048163	-1.001259
	N	3.050211	-1.016949	-0.215569
	N	1.793118	1.226938	1.607751
	N	2.989833	0.546258	1.764925
	C	-3.966344	0.476127	-1.453306
	C	-4.029529	-0.852475	-1.794799
	C	-3.158198	-1.510657	-0.937217
	C	-2.051280	4.207164	-0.356669
	C	-0.839098	4.680183	-0.791501
	C	-0.000079	3.577797	-0.775116
	C	-3.191856	1.813061	3.083569
	C	-2.379424	1.381179	4.115151
	C	-1.254230	0.825895	3.505927
	C	-0.116425	-2.296313	-2.612487
	C	-0.085620	-3.559116	-3.301482
	C	0.384413	-4.678005	-2.707288
	C	0.878343	-4.577191	-1.394501
	C	0.787138	-3.361690	-0.750304
	C	-0.589360	-1.134224	-3.251581
	C	-0.924695	-1.074636	-4.639773
	C	-1.373727	0.056554	-5.213267
	C	-1.557528	1.210454	-4.432068
	C	-1.198294	1.134366	-3.098176
	C	2.305317	-2.828948	2.899857
	C	1.076234	-3.343167	3.233789
	C	0.127804	-2.588286	2.534309
	C	3.753107	-1.874541	-1.002982
	C	3.630968	-1.430349	-2.313581
	C	2.805950	-0.307363	-2.280966
	C	3.861137	1.313376	2.471501

	C	3.225526	2.475467	2.813211
	C	1.930614	2.393143	2.251643
	B	-2.956220	1.866553	0.475463
	B	3.142847	-0.907941	1.340928
	H	-4.019777	2.444487	0.502250
	H	4.234937	-1.298972	1.685208
	H	-4.643149	-1.292356	-2.575289
	H	-0.596836	5.694662	-1.091505
	H	-2.567287	1.482251	5.179899
	H	-0.464996	-3.611631	-4.320682
	H	0.389434	-5.632396	-3.237154
	H	1.307765	-5.431344	-0.870891
	H	1.130880	-3.281248	0.276191
	H	-0.788767	-1.964563	-5.252852
	H	-1.605799	0.072064	-6.280658
	H	-1.943135	2.142980	-4.842187
	H	-1.297177	2.015240	-2.468209
	H	0.883315	-4.167574	3.914116
	H	4.082150	-1.885518	-3.190717
	H	3.640204	3.303353	3.381090
	H	4.328529	-2.688386	-0.574483
	H	2.422708	0.302531	-3.093515
	H	4.855107	0.946900	2.708092
	H	1.113935	3.109136	2.269393
	H	-0.955822	-2.664532	2.520463
	H	3.305278	-3.105372	3.217952
	H	-2.879359	-2.559772	-0.897871
	H	-4.509726	1.332939	-1.839092
	H	1.053915	3.520447	-1.038392
	H	-3.005540	4.703438	-0.210586
	H	-0.382083	0.372137	3.970726
	H	-4.149710	2.323132	3.082290

Table S5. Comparison of U(III) EPR g-values. Calculated values for the complexes reported herein are included in parentheses under the experimental values.

Complex	g_1	g_2	g_3	ref
Tp*UI_2 (**1**)	4.49 (4.84)	1.04 (0.81)	0.49 (0.15)	This work
Tp*$_2$UI (**2**)	4.59 (4.20)	1.42 (1.14)	0.66 (0.90)	This work
Tp*$_2$UBn (**3**)	4.83 (4.55)	1.45 (1.01)	0.57 (0.68)	This work
U[(μ-η^5:η^5-Cp)Re(BDI)]$_3$	3.04	~1.6	n.r.	25
[U(Cp^{tt})$_3$]	3.65	2.56	< 0.5	26
[(($^{t\cdot Bu}$ArO)$_3$tacn)U^{III}(^{Me}cy-C6)]·(^{Me}cy-C6)	2.89	1.86	0.93	27
Cp”$_3$U	3.03	2.31	<0.7	28
Cp”$_3$U•tBuNC	2.42	1.75	<0.7	28
Cp”$_3$U•CyNC	2.40	1.68	1.04	28
U(Bc^{Me})$_3$	2.57	1.03	n.r.	29
U(Bp^{Me})$_3$	2.62	1.76	n.r.	29

5. References

[1] E. M. Matson, W. P. Forrest, P. E. Fanwick and S. C. Bart, *J. Am. Chem. Soc.*, 2011, **133**, 4948-4954.

[2] Y. Sun, R. McDonald, J. Takats, V. W. Day and T. A. Eberspacher, *Inorg. Chem.*, 1994, **33**, 4433-4434.

[3] R. McDonald, Y. Sun, J. Takats, V. W. Day and T. A. Eberspracher, *J. Alloys Compd*, 1994, **213-214**, 8-10.

[4] S. J. Kraft, P. E. Fanwick and S. C. Bart, *Inorg. Chem.*, 2010, **49**, 1103-1110.

[5] Baerends, E. J.; Ziegler, T.; Atkins, A. J.; Autschbach, J.; Baseggio, O.; Bashford, D.; Bérces, A.; Bickelhaupt, F. M.; Bo, C.; Boerrigter, P. M.; Cavallo, L.; Daul, C.; Chong, D. P.; Chulhai, D. V.; Deng, L.; Dickson, R. M.; Dieterich, J. M.; Ellis, D. E.; Faassen, M. v.; Fan, L.; Fischer, T. H.; Guerra, C. F.; Franchini, M.; Ghysels, A.; Giammona, A.; Gisbergen, S. J. A. v.; Goez, A.; Götz, A. W.; Groeneveld, J. A.; Gritsenko, O. V.; Grüning, M.; Gusarov, S.; Harris, F. E.; Hoek, P. v. d.; Hu, Z.; Jacob, C. R.; Jacobsen, H.; Jensen, L.; Joubert, L.; Kaminski, J. W.; Kessel, G. v.; König, C.; Kootstra, F.; Kovalenko, A.; Krykunov, M. V.; Lenthe, E. v.; McCormack, D. A.; Michalak, A.; Mitoraj, M.; Morton, S. M.; Neugebauer, J.; Nicu, V. P.; Noodleman, L.; Osinga, V. P.; Patchkovskii, S.; Pavanello, M.; Peeples, C. A.; Philipsen, P. H. T.; Post, D.; Pye, C. C.; Ramanantoanina, H.; Ramos, P.; Ravenek, W.; Rodríguez, J. I.; Ros, P.; Rüger, R.; Schipper, P. R. T.; Schlüns, D.; Schoot, H. v.; Schreckenbach, G.; Seldenthuis, J. S.; Seth, M.; Snijders, J. G.; Solà, M.; Stener, M.; Swart, M.; Swerhone, D.; Tognetti, V.; Velde, G. t.; Vernooijs, P.; Versluis, L.; Visscher, L.; Visser, O.; Wang, F.; Wesolowski, T. A.; Wezenbeek, E. M. v.; Wiesenekker, G.; Wolff, S. K.; Woo, T. K.; Yakovlev, A. L.: Amsterdam Density Functional. 2017 ed.; SCM, Theoretical Chemistry, Vrije Universiteit Amsterdam, The Netherlands, **2017**.

[6] Perdew, J. P.; Burke, K.; Ernzerhof, M. Generalized Gradient Approximation Made Simple. *Phys. Rev. Lett.* **1996**, 77, 3865-3868.

[7] van Lenthe, E.; Ehlers, A. E.; Baerends, E. J. Geometry optimization in the Zero Order Regular Approximation for relativistic effects. *J. Chem. Phys.* **1999**, 110, 8943-8953.

[8] van Lenthe, E.; Baerends, E. J.; Snijders, J. G. Relativistic regular two-component Hamiltonians. *J. Chem. Phys.* **1993**, 99, 4597-4610.

[9] Grimme, S. Accurate Description of van der Waals Complexes by Density Functional Theory Including Empirical Corrections. *J. Comput. Chem.* **2004**, 25, 1463-1473.

[10] van Lenthe, E.; Baerends, E. J. Optimized Slater-type basis sets for the elements 1-118. *J. Comput. Chem.* **2003**, 24, 1142-1156.

[11] Glendening, E. D.; Landis, C. R.; Weinhold, F. NBO 6.0: Natural bond orbital analysis program. *J. Comput. Chem.* **2013**, 34, 1429-1437.

[12] Barone, V.; Cossi, M. Quantum Calculation of Molecular Energies and Energy Gradients in Solution by a Conductor Solvent Model. *J. Phys. Chem. A* **1998**, 102,

1995-2001.
[13] Martin, R. L. Natural transition orbitals. *J. Chem. Phys.* **2003**, 118, 4775-4777.
[14] Shao, Y.; Head-Gordon, M.; Krylov, A. I. The spin-flip approach within time dependent density functional theory: Theory and applications to diradicals. *J. Chem. Phys.* **2003**, 118, 4807-4818.
[15] Casanova, D.; Krylov, A. I. Spin-flip methods in quantum chemistry. *Phys. Chem. Chem. Phys.* **2020**, 22, 4326-4342.
[16] Delesma, F. A.; Geudtner, G.; Mejía-Rodríguez, D.; Patrizia C.; Köster, A. M. Range-Separated Hybrid Functionals with Variational Fitted Exact Exchange. *J. Chem. Theory Comput.* **2018**, 14, 5608-5616.
[17] Hirata, S.; Head-Gordon, M. Time-dependent density functional theory within the Tamm-Dancoff approximation. *Chem. Phys. Lett.* **1999**, 314, 291-299.
[18] Neese, F. The ORCA program system. Wiley Interdiscip. *Rev. Comput. Mol. Sci.* **2012**, 2, 73-78.
[19] Neese, F. Software update: the ORCA program system, version 4.0. *Wiley Interdiscip. Rev. Comput. Mol. Sci.* **2018**, 8, e1327.
[20] Cossi, M.; Rega, N.; Scalmani, G.; Barone, V. Energies, structures, and electronic properties of molecules in solution with the CPCM solvation model. *J. Comput. Chem.* **2003**, 24, 669-681.
[21] Neese, F.; Wennmohs, F.; Hansen, A.; Becker, U. Efficient, approximate and parallel Hartree-Fock and hybrid DFT calculations. A 'chain-of-spheres' algorithm for the Hartree-Fock exchange. *Chem. Phys.* **2009**, 356, 98-109.
[22] Galván, I. F.; Vacher, M.; Alavi, A.; Angeli, C.; Aquilante, F.; Autschbach, J.; Bao, J. J.; Bokarev, S. I.; Bogdanov, N. A.; Carlson, R. K.; Chibotaru, L. F.; Creutzberg, J.; Dattani, N.; Delcey, M. G.; Dong, S.; Dreuw, A.; Freitag, L.; Frutos, L. M.; Gagliardi, L.; Gendron, F.; Giussani, A.; Gonzalez, L.; Grell, G.; Guo, M.; Hoyer, C. E.; Johansson, M.; Keller, S.; Knecht, S.; Kovačević, G.; Källman, E.; Li Manni, G.; Lundberg, M.; Ma, Y.; Mai, S.; Malhado, J. P.; Malmqvist, P. A.; Marquetand, P.; Mewes, S. A.; Norell, J.; Olivucci, M.; Oppel, M.; Phung, Q. M.; Pierloot, K.; Plasser, F.; Reiher, M.; Sand, A. M.; Schapiro, I.; Sharma, P.; Stein, C. J.; Sørensen, L. K.; Truhlar, D. G.; Ugandi, M.; Ungur, L.; Valentini, A.; Vancoillie, S.; Veryazov, V.; Weser, O.; Wesołowski, T. A.; Widmark, P.-O.; Wouters, S.; Zech, A.; Zobel, J. P.; Lindh, R., 'OpenMolcas: From Source Code to Insight', *J. Chem. Theory Comput.* **2019**, 15, 5925–5964.
[19] Aquilante, F.; Autschbach, J.; Baiardi, A.; Battaglia, S.; Borin, V. A.; Chibotaru, L. F.; Conti, I.; De Vico, L.; Delcey, M.; Fdez. Galván, I.; Ferré, N.; Freitag, L.; Garavelli, M.; Gong X.; Knecht, S.; D. Larsson, E.; Lindh, R.; Lundberg, M.; Åke Malmqvist P.; Nenov A.; Norell, J.; Odelius, M.; Olivucci, M.; B. Pedersen, T.; Pedraza-González, L.; M. Phung, Q.; Pierloot, K.; Reiher, M.; Schapiro, I.; Segarra-Martí, J.; Francesco; Seijo, L.; Sen, S.; Sergentu, D.-C.; Stein, C. J.; Ungur1, L.; Vacher, M.; Valentini, A.; Veryazov, V. Modern quantum chemistry with [Open]Molcas. *J. Chem. Phys.* **2020**, 152, 214117.
[23] Wolf, A.; Reiher, M.; Hess, B.A., The generalized Douglas-Kroll transformation, *J. Chem. Phys.* **2002**, 117, 9215–9226.
[24] Roos, B. O.; Taylor, P. R.; Siegbahn, P. E. M., A Complete Active Space SCF

method (CASSCF) using a density matrix formulated super-CI approach, *Chem. Phys.* **1980**, 48, 157–173.
[25] M. A. Boreen, T. D. Lohrey, G. Rao, R. D. Britt, L. Maron and J. Arnold, *J. Am. Chem. Soc.*, 2019, **141**, 5144-5148.
[26] A. Formanuik, A.-M. Ariciu, F. Ortu, R. Beekmeyer, A. Kerridge, F. Tuna, E. J. L. McInnes and D. P. Mills, *Nat. Chem.*, 2017, **9**, 578-583.
[27] J. Jung, S. T. Löffler, J. Langmann, F. W. Heinemann, E. Bill, G. Bistoni, W. Scherer, M. Atanasov, K. Meyer and F. Neese, *J. Am. Chem. Soc.*, 2020, **142**, 1864-1870.
[28] W. W. Lukens, M. Speldrich, P. Yang, T. J. Duignan, J. Autschbach and P. Kögerler, *Dalton Trans.*, 2016, **45**, 11508-11521.
[29] K. R. Meihaus, S. G. Minasian, W. W. Lukens, S. A. Kozimor, D. K. Shuh, T. Tyliszczak and J. R. Long, *J. Am. Chem. Soc.*, 2014, **136**, 6056-6068.